

Recent Progress on Scanning Laser Epitaxy: A New Technique for Growing Single Crystal Superalloys

Michael Kirka, Rohan Bansal, and Suman Das

*Woodruff School of Mechanical Engineering, Georgia Institute of Technology
Atlanta, GA 30332-0405*

Abstract

This paper presents recent progress on scanning laser epitaxy, a laser manufacturing technique being developed for achieving single crystal growth in nickel-based superalloys. Investigations have been performed for creating monolithic deposits on like chemistry single-crystal nickel superalloy substrates. Progress in the areas of microstructure development and process control will be discussed in the context of repairing high-value single-crystal turbine engine components. This work is funded by the Office of Naval Research contract #N00173-07-1-G012.

Introduction

In the course of a single crystal (SX) airfoil's life, damage and wear occur on the leading tip in the amount of 0.5 to 1 mm, causing the turbine's performance to eventually deviate from design specifications. Once this occurs, the damaged airfoils must be replaced at a cost of several thousand dollars each. When considering that a turbine engine contains several hundred airfoils split between the various stages, the cost of replacement skyrockets to several hundreds of thousands of dollars. As a result there is a large interest in developing an additive process by which SX airfoils can be repaired and returned to service.

Prior processes such as laser engineered net shaping, laser scanning epitaxy, and cladding have attempted to restore single crystal airfoils to working condition. However, each approach was reported to be hindered by two main problems, crack formations in the added materials and stray grain formations. [1-5] This work focuses on developing a new process, scanning laser epitaxy (SLE), by which an arbitrary SX high value component can be repaired. Three thrusts define the scope of the work: 1) Investigate the fundamental sciences governing the additive material process 2) Develop the fundamental controls required to dictate the type, directionality, and scale of the deposited microstructure 3) Use the information gathered from thrusts 2 and 3 to develop a thermally controlled laser process. Below is outlined the progress to date in the experimental and control aspects of the work.

Experimental

Two nickel-based superalloys, MarM-247 (MARM) and CMSX-4 (CMSX) with compositions shown in Table 1 were chosen for experimentation based on their widespread usage in airfoils on jet powered aircraft and their solidification characteristics. MARM being polycrystalline and CMSX being SX capable. Both the MARM and CMSX powders were produced by Praxair Surface Technologies through an atomization process. Prior to usage the powders were heated in an argon purged vacuum oven for 24 hours at 200 °C. This was done in order to remove any moisture that may have been absorbed into the powder.

Polycrystalline MARM substrates of 3x0.75x0.1" and single crystal CMSX substrates of 1.4x0.4x0.1" were utilized as the base plates onto which the like chemistry powder was placed.

In each experiment 2mm of like chemistry powder was deposited onto the base plates, after being placed into a Terra Universal atmospheric glovebox. Following the powder placement, the glovebox was purged with argon until an oxygen content below 50 ppm was achieved. A 1064nm 2kW Nd:YAG laser beam was then focused through a Cambridge Technologies galvanometer scanner which delivered the beam to the substrate. For both the MARM and CMSX experiments a predetermined rectangular raster scan pattern was used in the absence of feedback controls.

Table 1: Chemical compositions (wt%) of MarM-247 and CMSX-4.

| | Cr | Co | Mo | Re | W | Al | Ti | Ta | Hf | B | C | Zr | Ni |
|--------------|-----|------|-----|------|-----|------|-----|-----|------|------|------|------|-----|
| MarM-247 [6] | 9.2 | 10.1 | 0.4 | ---- | 3.3 | 12.2 | 1.3 | 1.0 | 0.5 | 0.08 | 0.75 | 0.02 | Bal |
| CMSX-4 [7] | 7.6 | 9.3 | 0.4 | 1.0 | 2.0 | 12.6 | 1.3 | 2.2 | 0.03 | ---- | ---- | ---- | Bal |

The MARM parameter space included a laser power and scan speed range of 300-600W and 100-300 mm/s respectively and the CMSX parameter space included a scan speed range of 400-900 mm/s while the laser power was held constant at 500 W. In the case of the MARM experiments, two samples were produced for every parameter combination. One sample was analyzed in the as-processed condition and the second went through a post-process stress relief heat treatment in an argon purged tube furnace for 4 hours at 1060 °C.

Metallurgical analysis of the samples was conducted by cutting a lengthwise cross section through the center of the specimen and then cutting widthwise cross sections every 5mm. Grinding and polishing of the samples were conducted beginning with 80 Grit sanding disks and proceeding through 1200 Grit, after which polishing was followed with a 5 µm diamond suspension and 0.5 µm silica suspension. Following polishing the samples were etched in a solution composed of 20ml HCL, 40 ml Ethanol, and 4g CuSO₄ for 60 seconds. Metalographs were produced using a Leica DM6000 Optical Microscope equipped with an automated stage coupled to Leica Applications Suite software.

Results and Analysis

A typical as-processed MARM sample produced using a rectangular raster scan is shown in Figure 1. Figure 2a exhibits the typical as-processed microstructure result. In the particular parameter space examined, high power/low scan speeds yielded significant warping of the base substrate while low power/high scan speeds resulted in minimal meltback, thus a tradeoff will need to be made between meltback depth and substrate warping. Due to the polycrystalline nature of the MARM alloy base substrate, the added material exhibited a similar polycrystalline microstructure as can be noted in the micrographs in Figure 2a and b.

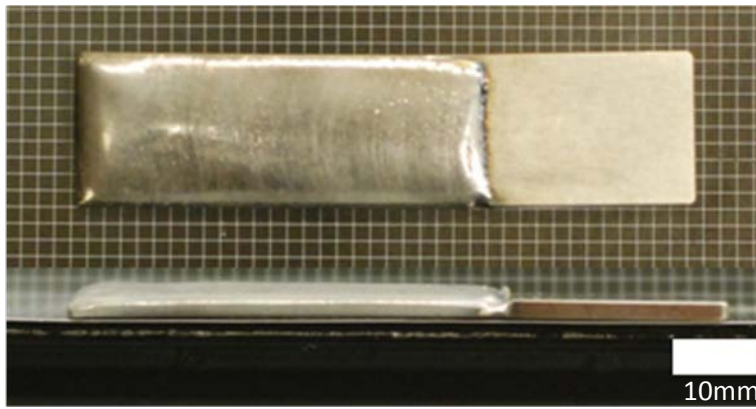


Figure 1: Top and side views of the typical as-processed MarM-247 sample.

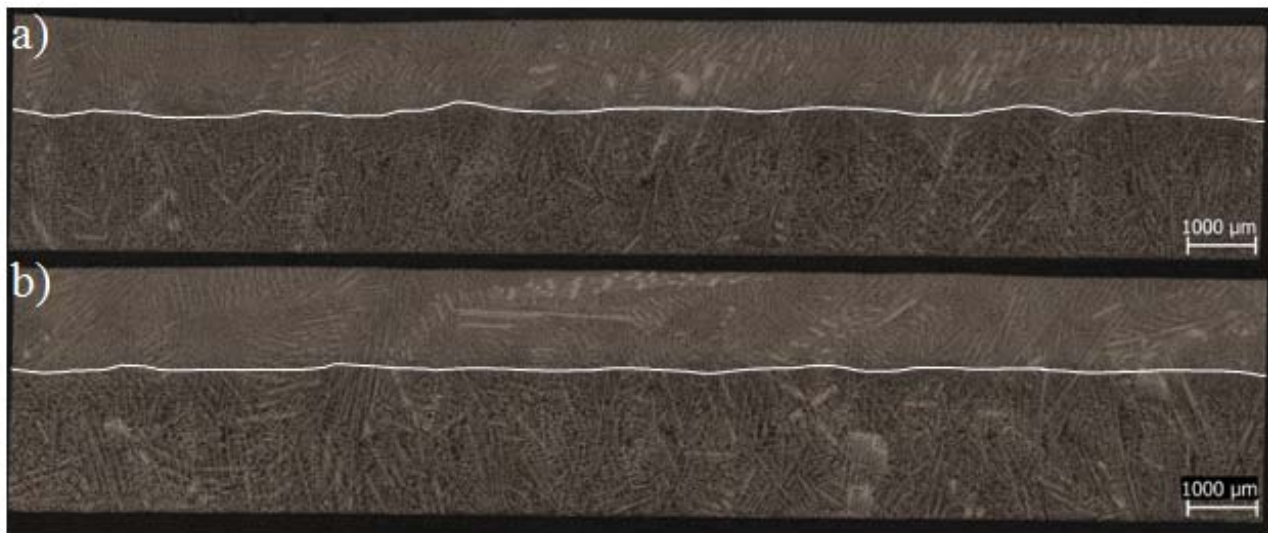


Figure 2: a) As-processed MARM longitudinal section view b) Heat treated MARM longitudinal section view. White line depicts the boundary between the base substrate and added material.

Further analysis of metalographs such as the one in Figure 2a of samples produced from parameters in the middle of the parameter space yielded three main observations and results 1) Fully dense deposits were achievable 2) Metallurgical bonds were formed between the melt and base substrate 3) Hot tearing, or stress cracking was not evident. In addition, the selection of samples that were given a stress relief heat treatment as a group did not exhibit cracking as a result of the heat treatment. An example of the microstructure of a heat treated sample is shown in Figure 2b.

A typical as-processed CMSX sample is presented in Figure 3. Unlike MARM, CMSX experiments revealed that the heat transfer within the melt pool and solidification geometry had a greater tendency to be influenced by surface tension gradients. This is particularly evident in the left hand side of the longitudinal micrograph (Figure 4) where the melt pool was initiated. Further, experiments conducted utilizing CMSX revealed five key observations upon microstructural analysis 1) Completely dense deposits were achievable 2) Metallurgical bonds were formed 3) Hot tearing was not evident in the as processed microstructure 4) Directionality of base microstructure was maintained 5) The primary dendrite arm spacing of the added material is on average 15 times finer than the primary dendrite spacing of the parent substrate.

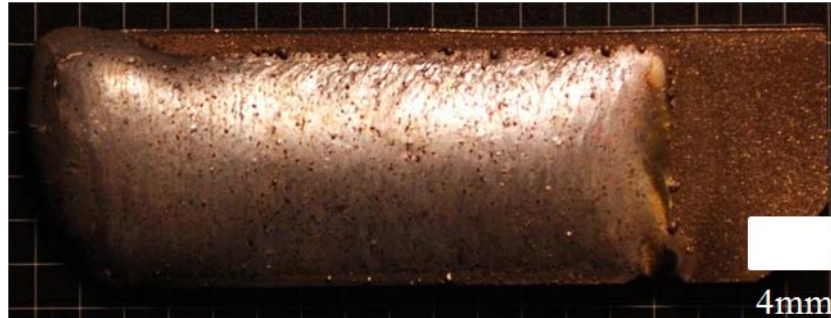


Figure 3: Top view of the typical as-processed CMSX-4 sample.

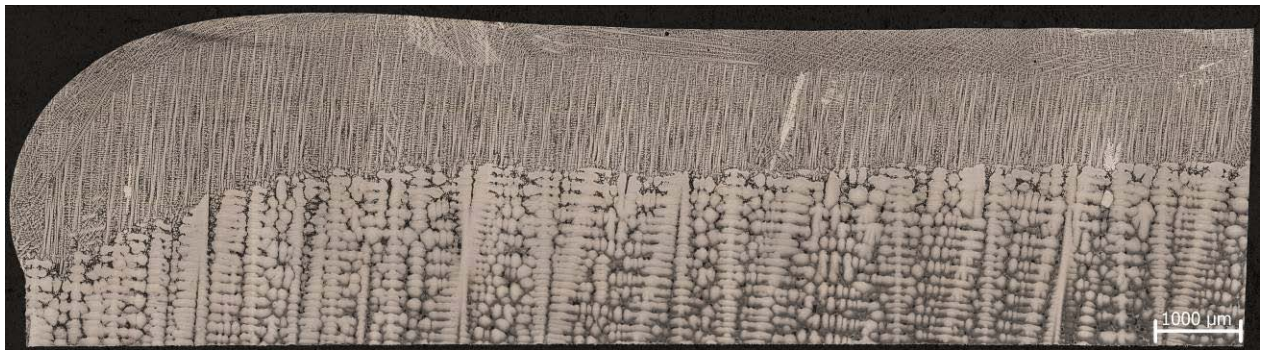


Figure 4: Longitudinal section of typical CMSX-4 sample; Note the melt boundary between the parent substrate and added material is given by the transition to the finer microstructure.

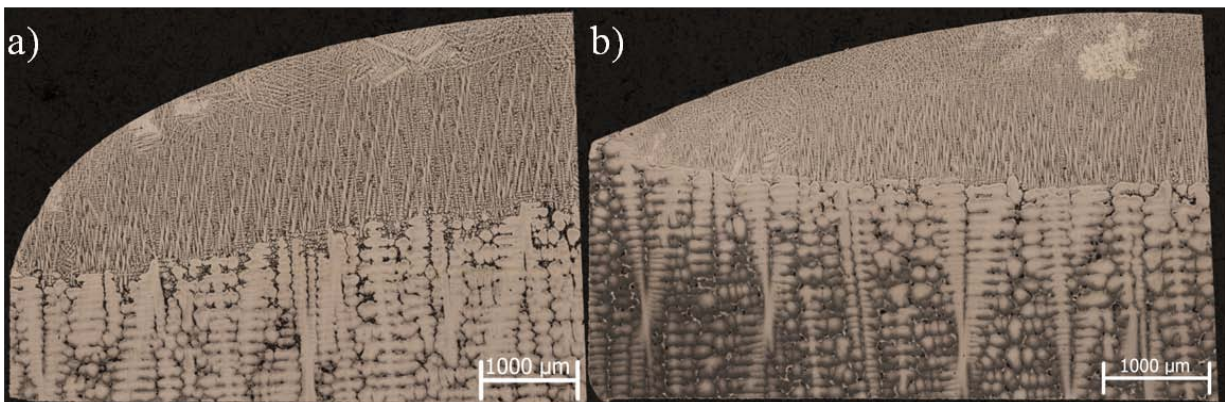


Figure 5: a) Width cross section of the typical CMSX-4 sample 5mm into the deposit. b) Width cross section of the typical CMSX-4 sample 15mm into the deposit. Note the melt boundary between the parent substrate and added material is given by the transition to the finer microstructure.

Of key importance in the processing of the CMSX samples is striking a balance between the substrate meltback and the net columnar to equiaxed grain growth ratio. If the meltback region is too shallow, delamination of the added material from the base substrate could occur. If the meltback region is too deep it increases the likelihood that the net growth of columnar grains (height of new columnar growth- height of meltback) will be less than the height of the equiaxed region, keeping a damaged airfoil in an unusable state.

For the particular parameter space where laser power is held constant at 500 W and only the scan speed is allowed to vary (420-840 mm/s), the average meltback was revealed to vary between 0.33 and 0.48 mm and the total amount of columnar growth was in the range of 0.30 and 0.55 mm. Generally, an inverse relationship between the net columnar growth and meltback was found (Figures 6 and 7).

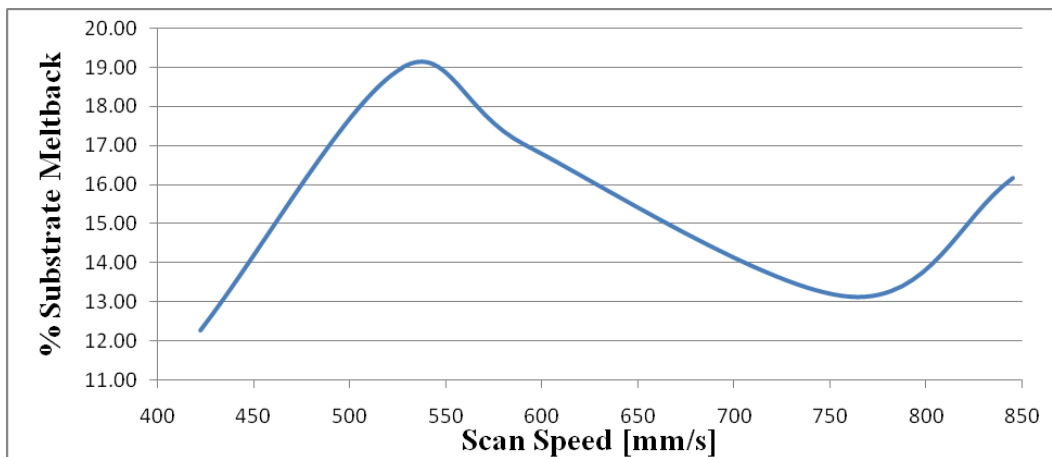


Figure 6: Experimentally determined relationship between percent of substrate meltback and laser scan speed while power held constant at 500W.

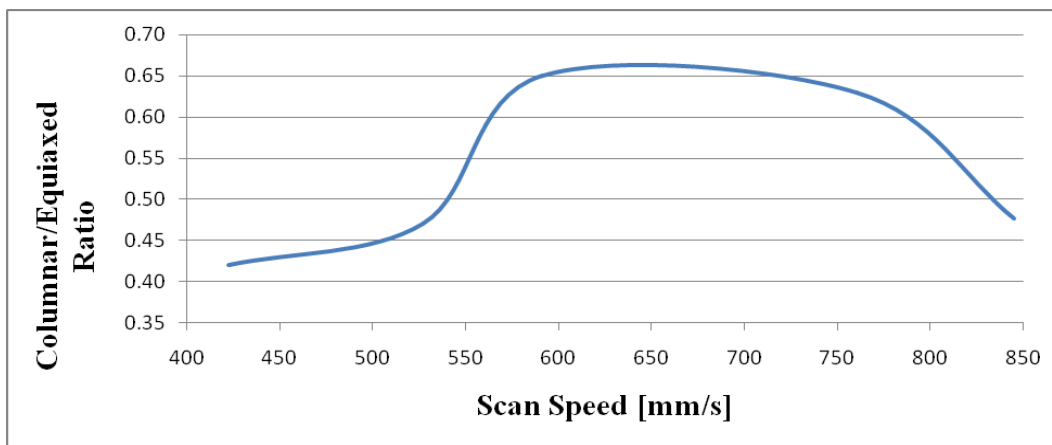


Figure 7: Experimentally determined relationship between the net columnar to equiaxed grain ratio and laser scan speed while power held constant at 500W.

From the representative longitudinal and widthwise cross sections in Figures 5a and b, the meltback can be observed to vary at the outer edges of the plate, with the trend being that as

the scan progresses further into the plate the amount of meltback decreases. This phenomena is attributed to the fact that melt pool is diffusing heat at a greater rate as it moves into the middle of the plate; the increasing thermal mass causes the temperature of the melt pool to decrease at a greater rate. It is this observation, which is evident throughout all the samples processed without thermal control, that shows that precise thermal control will be required in order to achieve the proper microstructure across a large deposit.

Process and Controls Overview

Due to the aforementioned experimental results, it has been determined that a robust temperature feedback control system will be required in order to generate the proper microstructure in the repair process. The primary components utilized in the experimental SLE feedback controls consist of a Hobart 2.2 kW 1064 nm Nd:YAG laser, a Cambridge Technologies galvanometer laser scanner, a Pyrofiber emissivity correcting pyrometer, an array of Omega K-type thermocouples, and a Coherent high power digital power meter. Additionally, a Sony video microscope with a bandpass optical filter is also included for post-processing analysis purposes. Figure 8 shows an overview of the SLE process control layout. The outputs of the system are XML format based laser positioning vectors and an analog laser power signal. The laser power, melt pool temperature, and the temperature of the substrate bottom are utilized as feedback signals.

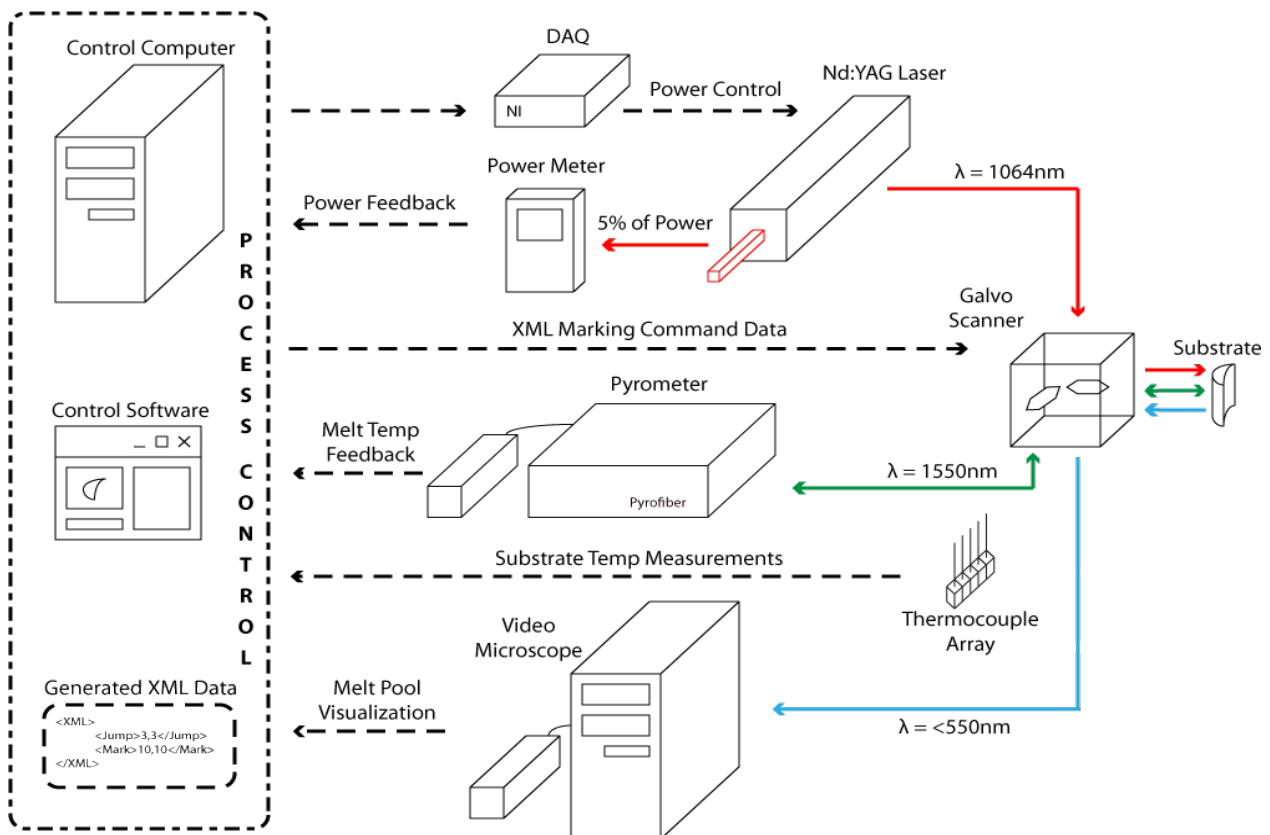


Figure 8: Process feedback control layout for the scanning laser epitaxy process.

As seen in the process controls layout in Figure 8, the galvanometer scanner is the central device. Through control software written in-house, XML marking commands are generated and drive the galvanometer scanners. With the ability for the scanner to receive commands in real-time, laser power, scan speed, and even scan path can be altered instantly to maintain preset parameters such as melt pool temperature.

To achieve control of the laser power via the process control software, the incident 1064nm Nd:YAG beam is split into two using a 95-5 beamsplitter optic, with 5% of the beam's power being diverted to the Coherent power meter which then relays the current power values to the process control software.

The melt temperature is calculated to within ± 4 °C by using an emissivity correcting pyrometer. The pyrometer uses a pulsed laser to calculate the reflectivity of the surface that it is measuring. The emissivity of the surface can then be calculated using Kirchhoff's law of thermal radiation and then used to correct the temperature readings based upon the changing emissivity of the melt as its temperature varies. [8] An array of K-type shrouded thermocouples and an Omega thermocouple DAQ are used to measure the temperature at the bottom of the substrate at six different points along its axis.

The versatility of the galvanometer setup in terms of response time and real-time controllability will allow for a robust feedback control system. Although most of the groundwork for implementing the proposed feedback control system has been laid, it has not yet been used experimentally. The determination of a proper mathematical model for the solidification process and the resulting feedback control scheme will comprise most of the future work involved in fully developing the scanning laser epitaxy process.

Conclusions

The results presented here within, report the progress that has been made in the development of scanning laser epitaxy; deposits of MarM-247 and CMSX-4 have been produced that are fully dense and metallurgically bonded to the base substrates. Optimization of the parameter space for both MARM and CMSX has been conducted, yielding desirable parameters for use in future work. Further, the results highlight the need for having a process feedback control system which can be exploited to maintain a constant meltback depth or maintain an optimized thermal gradient throughout the deposit.

Future work on scanning laser epitaxy will explore the effect of various power control schemes as well as different scan patterns such as contour scans or toroidal scans on melt pool behavior. In addition, work on joining numerical modeling results to those of analytical ones in a cohesive controls system is of great importance moving forward in developing the process of scanning laser epitaxy.

Acknowledgements

The authors of this paper would like to thank the Office of Naval Research for their support under contract #N00173-07-1-G012.

References

1. S. S. Babu, S. A. David, J.W. Park, and J. M. Vitek, "Joining of nickel-base superalloy single crystals", Proceedings of the Microstructure and Performance of Joints in High-Temperature Alloys, The Institute of Materials, Minerals, and Mining, London, UK (2002).
2. M. Gaumann et al., "Epitaxial laser metal forming: analysis of microstructure formation", Materials Science and Engineering A, Vol. 271, pp. 232-241 (1999).
3. M. G. Glavicic, K.A. Sargent, P.A. Kobryn and S.L. Semiatin, " The repair of single crystal nickel superalloy turbine blades using laser engineered net shape (LENS™) technology", Air Force Research Labs Document No. AFRL-ML-WP-TR-2003-4103.
4. J. W. Park, S. S. Babu, J. M. Vitek, E. A. Kenikm and S. A. David, "Stray grain formation in single crystal Ni-base superalloy welds", Journal of Applied Physics, Vol. 94, pp.4203-4209 (2003).
5. S. Mokadem, Epitaxial laser treatment of single crystal nickel-base superalloys, Ph.D. Dissertation, EPFL Lausanne, Switzerland (2004).
6. P. Caron and T. Khan, "Evolution of Ni-based superalloys for single crystal gas turbine blade applications" Aerospace Science and Technology, Vol. 3, pp. 513-523 (1999).
7. M. Donachie, Superalloys: A Technical Guide, ASM International, Materials Park, OH pp. 273 (2002).
8. Kral, J. and Matthews E. K. "Pyrolaser&Pyrofiber Infrared Temperature Measurement With Automatic Emissivity Correction." Paper presented at the International Fair of Metallurgy, Ostrava, Republic of Czechoslovakia, May (1996).